Agricultural and Forest Meteorology 386 (2026) 111238

Contents lists available at ScienceDirect

Agricultural and Forest Meteorology

journal homepage: www.elsevier.com/locate/agrformet

Decoding hotter-drought impacts on canopy activity and tree growth to diagnose forest die-off

J.Julio Camarero [a,*], Antonio Gazol [a], Cristina Valeriano [a,b], Michele Colangelo [c], Manuel Pizarro [a], Estér González de Andrés [a,b], Arens Pëto [a]

[a] Instituto Pirenaico de Ecología (IPE-CSIC), Avda. Montañana 1005, E-50192 Zaragoza, Spain
[b] Department of Physical Geography and Geoecology, Faculty of Science, Charles University, Albertov 6, Prague, Czech Republic
[c] Dipartimento di Scienze Agrarie, Forestali, Alimentari e Ambientali, Università della Basilicata, Potenza, Italy

ARTICLE INFO

Keywords:
Dendroecology
Die-off hotspot
EVI
Forest dieback
NDVI
Tree death

ABSTRACT

Decoding the long-term impacts of hotter droughts on canopy activity and growth provides information to forecast forest die-off leading to mortality hotspots. However, remotely sensed information often lacks field-based validation including long-term assessments of tree radial growth in those hotspots. To relieve this deficiency, we investigated climate data, canopy activity (NDVI, EVI) and radial growth in 45 die-off hotspots sampled across Spain and affecting six conifers (silver fir, Scots pine, Aleppo pine, maritime pine, stone pine, and Spanish juniper), and four broadleaves (European beech, pedunculate oak, downy oak, and holm oak). Hotter droughts, characterized by elevated evaporative water demand, are becoming more frequent in the study sites during the 21st century. Such warming and aridification started in the late 1990s and early 2000s and triggered several die-off hotspots, whose onset dates peaked in 1992, 2005, 2012, and 2017. In those sites, hotter droughts caused abrupt declines in canopy activity and radial growth. Year-to-year growth variability was more sensitive to drought than canopy greenness, and wetter sites showed the most negative growth trends. Drought constrained canopy activity and growth, which were more coupled in dry sites. The year of the strongest greenness loss and growth predated the observed die-off onset by six years, while abrupt growth reductions coincided with species-specific severe droughts such as 1986 (silver fir) or 2005 (Mediterranean pines). Both abrupt greenness loss and grow reductions were more common in recent years in drier sites as warming leads to more aridity. Forest mortality risk involves both site aridity and hotter-drought severity with tree-ring series representing promising data to forecast hotspot emergence.

1. Introduction

Warmer and drier conditions are driving aridification, negatively impacting some forests, causing die-off, growth decline and accelerating tree mortality (Hammond et al., 2022; Gazol et al., 2025a; Lu et al., 2026). These die-off and mortality hotspots have been described in all forested biomes in response to hotter droughts and under very different climate conditions (Allen et al., 2015; ITN, 2025). Such hotter droughts are a kind of compound climate extremes characterized by elevated temperatures, rising evaporative water demand (high vapour pressure deficit, VPD) and low precipitation (low soil moisture), and pose a high risk to forest existence and resilience (Zscheischler et al., 2018; Gazol and Camarero, 2022). First, a high VPD triggers stomatal closure and reduces photosynthesis rate, which could lead to carbon starvation (Grossiord et al., 2020). Second, soil dryness can induce hydraulic failure by restricting xylem and phloem flow and impairing meristem activity through low cell turgor and tissue dehydration (McDowell et al., 2008; Brodribb et al., 2020).

Different tree species and sites can be more or less vulnerable to atmospheric or soil drought and present contrasting dieback and mortality levels depending on local conditions and tolerance to elevated VPD and dry soil conditions (Greenwood et al., 2017). Some regions prone to hotter-drought forest damage have been intensively studied, such as the SW USA and Spain (Gazol et al., 2025a). Most studies on these die-off events have used the information provided by annual growth rings to build temporal frameworks assessing growth trends and

* Corresponding author.
E-mail addresses: jjcamarero@ipe.csic.es (J.Julio Camarero), agazol@ipe.csic.es (A. Gazol), valeriac@natur.cuni.cz (C. Valeriano), michele.colangelo@unibas.it (M. Colangelo), m.pizarro@csic.es (M. Pizarro), gonzalees@natur.cuni.cz (E. González de Andrés).

https://doi.org/10.1016/j.agrformet.2026.111238
Received 26 February 2026; Received in revised form 28 April 2026; Accepted 8 May 2026
Available online 18 May 2026

growth responsiveness to drought (e.g., Camarero et al., 2015; Valeriano et al., 2021; Martín-Benito et al., 2025). This research has used the temporal changes in the responses of trees to drought to attain new prospective information on how and when die-off and mortality hotspots occur. However, global synthesis following this approach and looking for early-warning signals in tree-ring data have found diverse results with higher predictive power only in some species and sites (Cailleret et al., 2019).

Tracking temporal variations of remotely sensed vegetation greenness allowed forecasting die-off events in Californian forests (Liu et al., 2019). Thus, combining temporal information on radial growth based on tree rings (dendroecology) with spatial information on canopy activity based on satellite-derived vegetation indices should improve our understanding of hotspot occurrence. Recently, Leduc et al. (2025) reviewed studies combining tree-ring and remote sensing information to assess disturbance impacts, including drought-induced forest damage. They reported that two of the most widely used vegetation indices are the Normalized Difference Vegetation Index (NDVI) and the Enhanced Vegetation Index (EVI). The NDVI measures the difference between near-infrared light, which vegetation reflects, and red light, which vegetation absorbs (Rouse et al., 1974), whereas the EVI improves sensitivity in regions with dense vegetation by including a canopy background adjustment and incorporating the blue band to correct for aerosol influences in the red band (Huete, 1997; Huete et al., 2002). However, the usefulness of each vegetation index may change between forest types, study cases, and drought severity timing. For example, NDVI data showed that greening trends dominated in Spanish forests due to ongoing encroachment, but some species and sites, such as maritime pine (*Pinus pinaster*) stands in xeric sites, presented a higher sensitivity to drought (Khoury and Coomes, 2020). Remarkably, this pine species presented severe die-off episodes in response to recent droughts and has been regarded as a "sentinel species" for detecting die-off and mortality hotspots (Camarero et al., 2026). In another case, EVI showed positive relationships with radial growth data in Pyrenean silver fir (*Abies alba*) hotspots (Crespo-Antia et al., 2024). In Europe, Senf et al. (2020) found that drought caused approximately 500,000 ha of unusually high forest mortality between 1987 and 2016 based on 30-m satellite-based canopy maps. Overall, remote sensing allows monitoring forest condition due to its continuous coverage in space and time, but predicting tree drought mortality is complicated because of different species' vulnerability to water shortage and site factors (Trugman et al., 2021). We therefore propose that complementary tree-ring and remote sensing data can improve the detection of hotspots. This is supported by studies showing a reduction in growth and greenness resilience of hotspots and forests associated to climate change (DeSoto et al., 2020; Forzieri et al., 2022).

This study addresses a critical research gap in forest die-off research, i.e., the integration of long-term, field-based dendroecological data with satellite-derived vegetation indices (NDVI, EVI), to understand temporal processes in die-off and mortality hotspots. We aimed to characterize and decode hotter drought impacts on canopy activity and radial growth, and how they are linked to climate variability. We addressed these issues by: (i) compiling and sampling a unique dataset of die-off and mortality hotspots in 45 sites located across Spain spanning a wide range of climate and soil conditions, and affecting different tree and shrub species, and (ii) evaluating the relationships between climate and growth variability, and canopy activity to better understand tree drought mortality. We sampled those mortality hotspots, dated the most recent year of the die-off onset, retrieved climate data and drought indices, and used remote sensing and dendrochronology to measure growth patterns and changes in canopy cover and greenness for the period 1984–2023. Specifically, we (i) quantified the temporal trends in climate (temperature, precipitation, vapor pressure deficit -VPD, and a drought index), canopy activity and radial growth before the mortality event, (ii) quantified the year-to-year variability in growth and canopy activity, and (iii) computed growth trends and drought-growth relationships in forests showing die-off (see also Gazol et al., 2025b). We expected that growth and canopy activity would be co-limited by low soil moisture and warm summer temperatures, i.e., hotter droughts, resulting in heightened vulnerability and hotspot emergence. We also hypothesized that growth measures at the tree and stand levels of the most impacted species will be more responsive to drought severity than changes in canopy cover and activity assessed at a similar spatial scale (0.5–1.5 ha). At this scale, remotely-sensed signals integrate contributions from coexisting species and different stand structures.

2. Material and methods

2.1. Study sites

We sampled 45 mortality hotspots across Spain in which our research group has investigated drought-induced forest die-off over the past two decades (Fig. S1, Table 1). The plot size of the sampled stands ranged between ca. 5000 to 20,000 m^2 depending on the height of sampled trees or shrubs. The percent cover of the species from which tree cores were taken varied from 90 % in the humid sites to 40 % in the driest sites. The year of the onset of die-off was considered when abnormally high mortality and defoliation levels were first observed by forest managers or by us after severe hot droughts. Mortality affected 11–70 % of sampled trees of the dominant species in most sites (cf. Camarero et al., 2015, 2020a, 2026; Valeriano et al., 2021). The database encompasses a wide variety of climate conditions (Fig. S2), tree species and the shrub *Juniperus phoenicea* L. We calculated the aridity index (ratio between precipitation and potential evapotranspiration) at a ca. 1-km spatial resolution to characterize site dryness (Zomer et al., 2022). Most sites ($n = 31$) were located in drylands and showed aridity indices (AI) lower than 0.65 (Mirzabaev et al., 2022). A total of 10 woody species (6 gymnosperms and 4 angiosperms) were considered, including silver fir (*Abies alba* Mill.) and Scots pine (*Pinus sylvestris* L.), which were the most studied species. Accordingly, conifer sites were very represented ($n = 37$ sites), whereas broadleaf forests (European beech, *Fagus sylvatica* L.; pedunculate oak, *Quercus robur* L.; downy oak, *Quercus pubescens* Willd.) were less frequent ($n = 12$) and occurred in humid sites with AI > 0.65. The driest sites (AI < 0.3) were dominated by Mediterranean pines such as Aleppo pine (*Pinus halepensis* Mill.), maritime pine (*Pinus pinaster* Ait.) and stone pine (*Pinus pinea* L.), but also by broadleaves (holm oak, *Quercus ilex* L.). In all study sites, the dominant species showing dieback was sampled for tree-ring analyses.

All sites correspond to natural stands, except five sites which are pine plantations (*P. sylvestris*, Hereña; *P. pinaster*, Aladrén and Herrera de los Navarros; *P. pinea*, Arenys de Munt; *P. halepensis*, Málaga). The last site corresponds to urban forests showing ongoing die-off (Cachinero et al., 2025), whereas the first site is an old, naturalized plantation. Few sites have experienced recent disturbances other than hotter droughts, except two *P. halepensis* sites (Sierra de Luna, Zuera), which were affected by wildfires before the 1980s (see also Fig. S1). In any case, we avoided sampling stands affected by wildfires or trees and stands presenting post-fire injury, including stem scars or crown scorch. Most sites have not been harvested or logged after the die-off damage, except for two *P. pinea* sites located near urban or recreational areas of big cities, such as Barcelona (Arenys de Munt site) and Madrid (Pelayos site). Finally, tree-to-tree competition is low in many sites, particularly those from dry areas, which are open stands (e.g., Miedes de Aragón, a *P. pinaster* site; cf. Camarero et al., 2026).

2.2. Climate data

We retrieved ~4-km spatial resolution climate data from the Terraclimate dataset and for the period 1960–2024 (Abatzoglou et al. 2018) from each site using the package TerraclimateR (Selker, 2025) in the R statistical environment (R Core Team, 2025). Specifically, monthly values of the following variables were obtained: mean maximum and

Table 1
Characteristics of the studied die-off mortality hotspots. AI is the aridity index.

Site	Dominant species	Secondary species	Latitude (°N)	Longitude (°, -W, +E)	Elevation (m a.s.l.)	AI	Year of die-off onset
Beluntza	*Quercus robur*	*Fagus sylvatica*	42.950	−2.888	620	0.860	2017
Aramendia	*Quercus pubescens*	*Quercus faginea*	42.717	−2.111	675	0.647	2017
Alsasua	*Quercus robur*	*Fagus sylvatica*	42.897	−2.084	615	0.889	2017
Galdeano	*Quercus pubescens*	*Fagus sylvatica*	42.735	−2.107	649	0.739	2017
Lokiz	*Fagus sylvatica*	*Quercus pubescens*	42.717	−2.170	989	0.755	2016
Eraso	*Fagus sylvatica*	*Quercus robur*	42.953	−1.801	547	0.810	2017
Opakua	*Fagus sylvatica*	*Quercus robur*	42.799	−2.331	1020	0.828	2005
Albarún	*Abies alba*	*Quercus subpyrenaica*	42.606	−0.504	1470	0.698	1995
Castiello de Jaca	*Abies alba*	*Q. subpyrenaica*	42.639	−0.534	1142	0.608	1992
Basari	*Abies alba*	*Fagus sylvatica*	42.727	−0.973	719	0.610	1992
Burgi	*Abies alba*	*Fagus sylvatica*	42.727	−0.974	765	0.618	1992
Fago	*Abies alba*	*Fagus sylvatica*	42.724	−0.883	957	0.647	1995
Salvatierra de Escá	*Abies alba*	*Pinus sylvestris*	42.732	−0.916	827	0.627	1992
Barranco del Chate	*Abies alba*	*Fagus sylvatica*	42.570	−0.080	991	0.620	1992
Lopetón	*Abies alba*	*Fagus sylvatica*	42.760	−0.850	1039	0.665	1992
Lizara	*Abies alba*	*Fagus sylvatica*	42.760	−0.630	1370	0.957	1992
Paco Ezpela	*Abies alba*	*Fagus sylvatica*	42.740	−0.830	1244	0.683	1992
Paco Mayor	*Abies alba*	*Fagus sylvatica*	42.710	−0.650	1285	0.718	1992
Peña Oroel	*Abies alba*	*Pinus sylvestris*	42.520	−0.540	1733	0.710	1992
San Juan de la Peña	*Abies alba*	*Pinus sylvestris*	42.520	−0.700	991	0.556	1992
Roncal	*Pinus sylvestris*	*Fagus sylvatica*	42.802	−0.942	801	0.682	2022
Corbalán	*Pinus sylvestris*	*Pinus nigra*	40.442	−0.988	1209	0.329	2005
Adobes	*Pinus sylvestris*	*Pinus nigra*	40.667	−1.687	1429	0.417	2015
Traid	*Pinus sylvestris*	*Pinus nigra*	40.661	−1.781	1457	0.426	2015
Prades	*Pinus sylvestris*	*Quercus ilex*	41.337	1.015	921	0.500	2022
Calomarde	*Pinus sylvestris*	*Quercus faginea*	40.370	−1.560	1340	0.384	2012
Guadarrama	*Pinus sylvestris*	*Pinus nigra*	40.667	−4.155	1276	0.450	2012
Hereña	*Pinus sylvestris*	*Fagus sylvatica*	42.770	−2.920	580	0.668	2012
Miedes de Aragón	*Pinus pinaster*	*Quercus ilex*	41.269	−1.434	986	0.299	2017
Orera	*Pinus pinaster*	*Quercus ilex*	41.317	−1.457	864	0.295	2017
Aladrén	*Pinus pinaster*	*Quercus ilex*	41.240	−1.195	1014	0.296	2020
Herrera de los Navarros	*Pinus pinaster*	*Quercus ilex*	41.160	−1.096	947	0.307	2022
Arenys de Munt	*Pinus pinea*	*Quercus suber*	41.612	2.624	98	0.573	2015
Almorox	*Pinus pinea*	*Quercus ilex*	40.275	−4.366	692	0.231	2015
Pelayos	*Pinus pinea*	*Quercus ilex*	40.340	−4.370	823	0.247	2015
Navas	*Pinus pinea*	*Quercus ilex*	40.414	−4.312	681	0.230	2015
Zuera	*Pinus halepensis*	*Quercus ilex*	41.981	−0.909	571	0.289	2012
Lanaja	*Pinus halepensis*	*Quercus coccifera*	41.753	−0.431	365	0.273	2012
Peñaflor	*Pinus halepensis*	*Juniperus thurifera*	41.781	−0.725	365	0.230	2012
Sierra de Luna	*Pinus halepensis*	*Quercus coccifera*	41.980	−0.840	493	0.269	2012
Málaga	*Pinus halepensis*	*Ceratonia siliqua*	36.725	−4.386	71	0.213	2022
Valcuerna	*Juniperus phoenicea*	*Pistacia lentiscus*	41.425	0.093	136	0.232	2012
Yaso	*Juniperus phoenicea*	*Quercus coccifera*	42.208	−0.126	717	0.371	2005
Doñana	*Juniperus phoenicea*	*Pinus pinea*	36.967	−6.466	8	0.302	2005
Paniza	*Quercus ilex*	*Quercus faginea*	41.273	−1.249	810	0.269	2022

minimum temperatures, precipitation, climate water deficit (difference between reference and actual evapotranspiration), soil moisture, VPD, and the Palmer Drought Severity Index (PDSI) (see Table S1). We acknowledge that the spatial scale of climate data is larger than that of NDVI-EVI and tree-ring data, but we aimed to represent the impact of regional droughts and climate data were not available at finer resolution for all sites.

The difference between precipitation and potential evapotranspiration was used to quantify the cumulative water balance, which was expressed as the Standardized Precipitation-Evapotranspiration Index (SPEI; Vicente-Serrano et al., 2010). The SPEI is a multi-scalar index based on the difference between the water supply (precipitation) and the demand (evapotranspiration) that has been widely used to quantify the impact of drought severity on forest growth and canopy activity (Pasho et al., 2011). Positive values correspond to wetter than normal conditions, while negative values indicate drier than normal conditions. The SPEI reflects better changes in drought severity across temporal scales than the PDSI. We used the R package SPEI (Beguería and Vicente-Serrano, 2023) to obtain monthly values of the SPEI drought index from 1 to 48 months. We defined as hotter-drought years those in which the VPD of May, June or July was above the 90 % percentile and the SPEI value for the month of July at 3-, 6- or 12-month-long scales was lower than −1.28, equivalent to a return period of 10 years. That is, we selected as hotter-drought events those years in which at least one value of VPD during the selected months (May to July) and one scale of SPEI during the month of July (3-, 6- or 12-month-long scales) were above the corresponding 90 % percentile.

Lastly, nineteen bioclimatic variables were obtained for each site to represent local bioclimatic conditions (see Table S2). These variables corresponded to the WorldClim database (www.worldclim.org). The bioclimatic variables were derived from monthly temperature and precipitation records for the period 1970–2000 and were obtained at ca. 1-km spatial resolution. These bioclimate variables provide information on seasonal climate means, seasonality, and climate extremes (Hijmans et al., 2005; Fick and Hijmans, 2017). The geodata (Hijmans et al., 2024) and raster (Hijmans, 2024) R packages were used to download bioclimatic data.

2.3. Remote sensing data

We used the Landtrend-CSIC application (https://landtrend.csic.es/ltr-vegchanges/; Pizarro, 2024) to obtain annual NDVI and EVI series (e.g., Fig. S3) for each studied site at a 30 m resolution for the period 1984–2023. We used data from the available Landsat-5 TM, Landsat-7 ETM+, Landsat-8 OLI and Landsat-9 OLI-2 images, ensuring high-quality data for large spatial extents over time. Selected images

were atmospherically corrected based on surface reflectance values (see more details in Crespo-Antia et al., 2024). The original 16-composite series of NDVI and EVI were transformed into annual averages. Data were processed in Google Earth Engine (GEE) which included rigorous filtering of clouds, shadows, and snow using the Fmask algorithm, ensuring that only atmospherically clean observations were included in the analysis. For the assembly of the annual composites, the medoid algorithm was used, defined as a multidimensional analogue of the median that selects the real pixel whose Euclidean distance is minimal from the median of all bands (Flood, 2013). This method ensures that the resulting value is a real physical observation captured by the sensor on a single date, maintaining the integrity of the spectral signatures and high temporal coherence and robustness against outliers (Roberts et al., 2017). We focused on stands where die-off intensity was high (10–30 % dead trees or with crown defoliation > 50 %) and obtained NDVI and EVI data for nine 30-m pixels (8100 m^2) arranged as a square grid or lattice shape and centered in each stand. The Landtrend algorithm performs a temporal segmentation of the NDVI or EVI data by fitting straight line segments to show trends and eliminate the noise (Kennedy et al., 2010). We obtained detrended NDVI and EVI residuals (NDVIr and EVIr, respectively) by subtracting observed NDVI or EVI data from fitted linear regressions (Figs. S4 and S5). The final series included NDVI, NDVIr, EVI and EVIr annual data.

We considered the year of abrupt EVI loss which occurred shortly before the die-off year as a proxy of hotspot occurrence. We selected the EVI to avoid the saturation problem in dense forests associated with the NDVI and because of the higher accuracy of the EVI to pinpoint die-off events (e.g., Crespo-Antia et al., 2024). This abrupt loss in canopy activity was detected using the "Continuous Change Detection and Classification" (CCDC) algorithm and analyzing time series of NDVI and EVI at 16-day intervals. Shortly, the CCDC detects breakpoints in the time series through temporal segmentation (Zhu and Woodcock, 2014; Zhu, 2017). We applied a 0.27 high-magnitude threshold to detect years with abrupt EVI losses, indicating major disturbances related to drought impacts, and the recovery phase (post-disturbance regrowth) corresponded to EVI > 0.29 afterwards. This threshold was based on previous analyses showing that similar relative changes in EVI corresponded to drought-induced mortality (Crespo-Antia et al., 2024).

2.4. Field sampling

In each site, a variable number of living adult trees or shrubs (from 15 to 80, mean = 35 individuals per site), representing the stand situation in terms of canopy defoliation, were sampled in a rectangular plot of 0.5–1.5 ha by extracting cores at a height of 1.3 m (dbh, diameter at breast height) perpendicular to the maximum slope using a Pressler increment borer. In the case of *J. phoenicea* and small trees (e.g., *Q. ilex*), basal stem cross-sections were cut using a saw. The wood samples, either cores or disks, were processed using dendrochronological methods (Fritts, 1976). Cores were air-dried, glued onto wooden supports, and carefully sanded with progressively finer-grain sandpaper until ring boundaries were clearly visible. Then, they were scanned at 2400 dpi resolution and visually cross-dated. Ring widths were measured with a 0.01 mm resolution using scanned images and the CooRecorder-CDendro software (Maxwell and Larsson, 2021). The quality of cross-dating was checked using the COFECHA software, which calculates moving correlations between individual series of ring-width values and the mean sites series (Holmes, 1983).

2.5. Processing tree-ring data

To quantify growth trajectories, tree-ring width series were converted into basal area increment (BAI), which reflects changes in stem area. The BAI was calculated as:

$$BAI = \pi \times \left(R_t^{\,2} - R_{t-1}^{\,2}\right) \quad (1)$$

where R_t and $R_{t\text{-}1}$ are the radii measured in years t and t-1, which correspond to the cumulative sums of annual ring widths until years t and t-1, respectively.

We calculated negative pointer years to reflect abrupt growth reductions potentially caused by droughts (Schweingruber et al., 1990). They were calculated for each site using the relative growth change method. Negative pointer years were defined as years in which at least 75 % of trees showed growth reductions higher than 40 % compared to the three preceding years. The negative pointer years were calculated using the pointRes R package (van der Maaten-Theunissen et al., 2015, 2021). Analogously to the selection of the year with highest EVI loss which occurred proximate to the die-off event, we selected in each site the last year with negative pointer years up to the die-off year as a growth proxy of hotspot emergence.

To assess the relationships between drought severity (SPEI) and year-to-year growth variability, tree-ring width series were detrended and standardized to obtain ring-width indices (RWI). Size-related changes in ring-width trends were removed by fitting a 25-year smoothing spline to each individual ring-width series. Dimensionless ring-width indices were then calculated as the ratio between measured values and their corresponding fitted spline values (Fritts, 1976). Then, autoregressive models were fitted to obtain pre-whitened or residual series of ring-width indices, which were averaged for each site using robust bi-weight means. Similarly, NDVI series in each site were detrended using 25-year smoothing spline to compare growth (RWI) and NDVI variability through Pearson correlation analyses. NDVI was used instead of EVI for exploratory analyses because higher correlations were obtained for NDVIr-RWI. Two tree-ring statistics were calculated to characterize the growth series: AR1, the first-order autocorrelation of ring-width series; and rbar, the mean correlation between the individual indexed series within each site. We also calculated the Expressed Population Signal to assess the coherence of site chronologies (Wigley et al., 1984). We calculated Pearson correlation coefficients between RWI, NDVIr and the SPEI. Correlations were obtained from September of the previous year of growth (t-1) to September of the current year (t). A permutation test with 1000 permutations was used to establish the significance ($p < 0.05$) of each correlation coefficient. Analyses were performed at scales from 1 to 48 months during the period 1984–2023 using 25-year moving windows. Note that the end year can vary between sites in the case of the RWI due to data availability. For each site, we selected the scale and period at which the maximum correlation between the RWI or NDVIr and the SPEI drought index was found. Analyses concerning tree-ring data were done using the dplR (Bunn, 2008, 2010; Bunn et al., 2025) and treeclim (Zang and Biondi, 2015) packages. All analyses were carried out using the R statistical program (R Core Team, 2025).

3. Results

3.1. Hotspot occurrence: climate triggers and event years

In the 45 mortality hotspots analyzed, climate conditions have evolved towards warmer and drier conditions. As a result, the occurrence of hotter droughts has increased (Fig. 1). Hotter droughts have occurred in recent years including 2019 (37 sites) and 2022 (43 sites), but also previously (1995, 40 sites; 2005, 41 sites). The most frequently dated die-off year was 1992 (11 events), followed by 2017, 2012 and 2005 (7 events each one), 2022, 2016, 2015, and 1995 (2 events each one), and 2019 (1 event; Table 1). It is important to note that hot and dry years, separately and not leading to compound events, were frequent in the past decade. Particularly, the year 2012 was characterized by very dry conditions but not so elevated temperatures, leading to a lower incidence of hotter droughts (28 sites), and the year 1986 was characterized by very dry conditions (31 sites) but much lower temperatures than in recent years (Fig. 1).

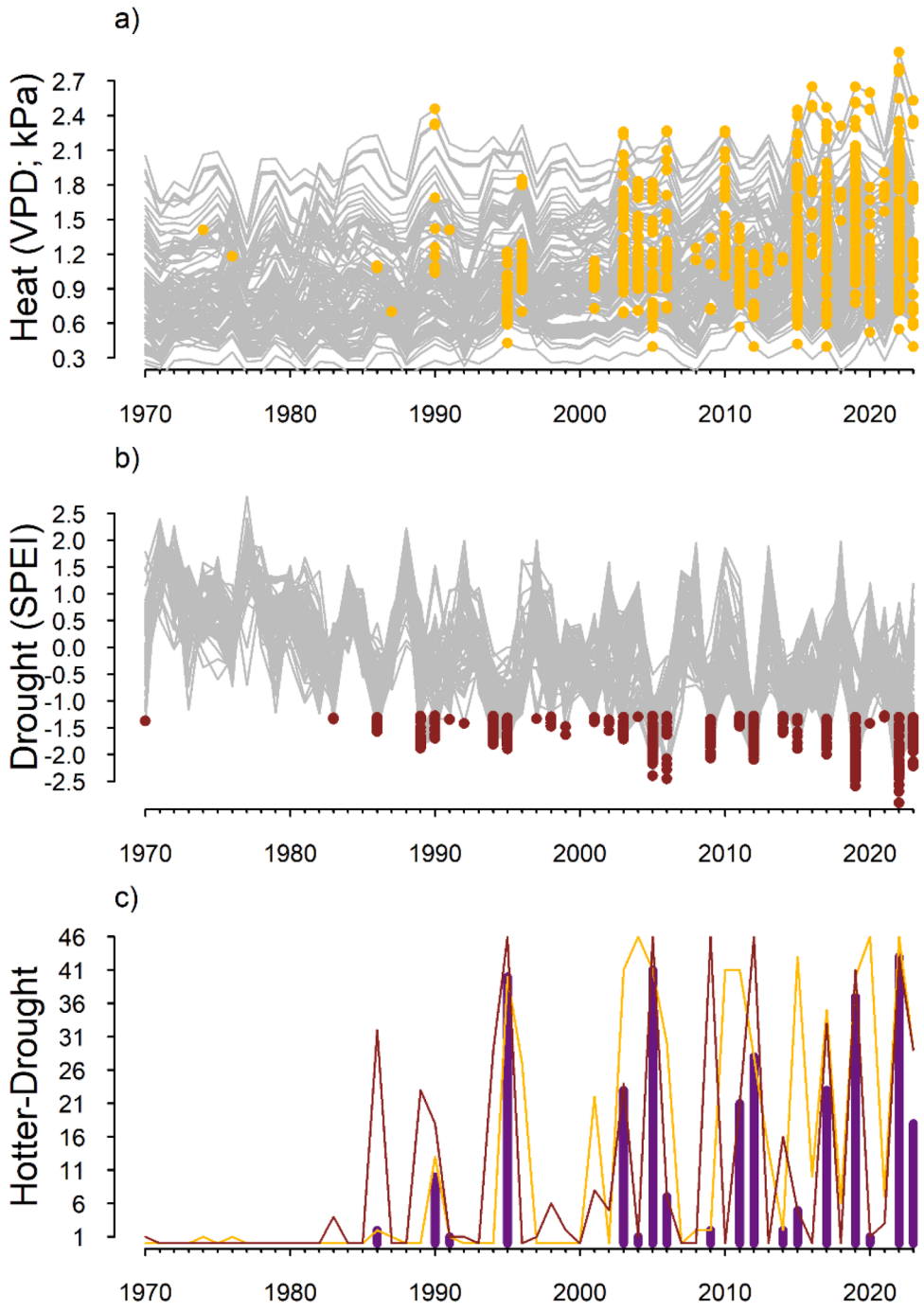

Fig. 1. Heat, drought and hotter drought changing in mortality hotspots. Changes in May to July VPD (heat stress) across the 45 mortality hotspots studied (a) with grey lines indicating the site observations and orange dots the years in which abnormally high values (above 90 % percentile) were found. (b) Changes in the July SPEI drought index with brown dots indicating dry years (drought stress). (c) Number of sites (purple bars) displaying a combination of heat and drought values, i.e., hotter droughts, in each year, as well as very hot (orange line) and very dry (brown line) years.

3.2. Values and trends of vegetation and growth in hotspots

The mean NDVI and EVI values of hotspots were 0.60 and 1.57, respectively, during the period 1984–2023 (Table S4). The mean BAI was 6.07 $cm^2\ yr^{-1}$. The mean NDVI, EVI and BAI trends were 0.0036 yr^{-1}, 0.0032 yr^{-1}, and −0.00087 $cm^2\ yr^{-2}$. The mean AR1 and rbar values were 0.32 and 0.41, in that order. The EPS values ranged 0.76–0.99 (mean = 0.94). The NDVI and BAI site values were positively correlated, albeit the strongest correlations were found between NDVIr and RWI, whereas the NDVI and BAI trends showed a negative correlation (Fig. S6). Drier sites showed lower BAI values, but higher AR1 (Fig. S7). NDVI increased as soil moisture did, but decreased as rbar increased (Fig. S8). The positive NDVIr-RWI correlations increased in dry sites and as AR1 did (Fig. S9).

Out of the 45 sites studied, 40 % of them showed significant ($p < 0.05$) negative BAI trends after 1980, whereas 29 % of them showed positive and significant BAI trends. Thus, negative growth trajectories prevailed in mortality hotspots despite increasing NDVI (Fig. 2**a**). Narrow growth rings, indicating low growth rates, were common in dry years such as 1986, 1995, 2005 and 2012 (Fig. 2**b**).

The BAI trend decreased in the wettest sites (Fig. 3**a**), whereas the sensitivity to drought, measured as the maximum correlations between

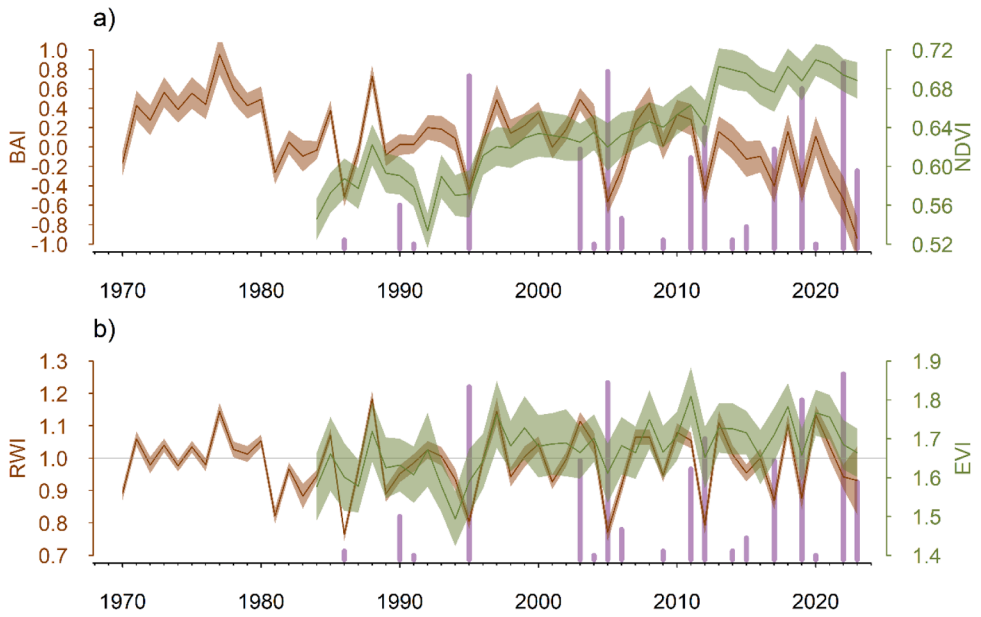

Fig. 2. Growth trends and variability in mortality hotspots. (a) Standardized mean basal area increments (BAI, brown lines -left *y* axis) and annual NDVI (green lines -right *y* axis) across sites and their standard errors are displayed together with the occurrence of hotter droughts (purple bars; the height of the bar is proportional to the number of sites; see Fig. 1**c**). (b) Ring-width indices (RWI, brown lines -left *y* axis) and EVI (green lines, -right *y* axis), and their corresponding standard errors.

RWI and the SPEI, increased as site aridity did (Fig. 3**b**).

The coupling between canopy activity and growth variability, measured as correlations between detrended NDVI and RWI, increased as site aridity did, i.e., it was more positive in dry sites (Fig. 4).

When relating climate, vegetation indices and growth metrics, the most numerous significant correlations were positive and corresponded to growth variables (BAI, RWI) and PDSI, followed by thermal variables (maximum temperature, VPD) and NDVI (Fig. S10). The highest correlations with climate variables corresponded to growth variables (BAI, RWI) and climate variables reflecting water availability, including the PDSI, soil moisture, and precipitation. Growth (BAI) decreased as VPD and the water deficit increased.

When relating the SPEI calculated at different temporal scales, vegetation indices and growth metrics, the number of significant positive correlations peaked for the 9- and 12-month-long SPEI values and RWI (Fig. S11), such growth responsiveness to drought increased as site aridity did (Fig. S12). The maximum correlation was found again between the 9- and 12-month-long SPEI values and RWI (Fig. S13).

3.4. Understanding hotspot occurrence based on drops in canopy activity and growth

The year of abrupt EVI loss increased as site aridity did (Fig. 5**a**). A similar response was found for tree growth data because negative pointer years were more frequent in wet sites (e.g., silver fir forests) from the 1980s to the 2000s, and in dry sites (e.g., Mediterranean pine forests) during the 2000s to the 2020s (Fig. 5**b**). In mountain cool-wet silver fir forests, most years of abrupt EVI loss occurred from 1990 to 1997, whereas they occurred from 2000 to 2010 in warm-dry lowland forests (e.g., Aleppo pine, maritime pine and stone pine sites). Scots pine hotspots showed sharp EVI drops from 1995 to 2007. Abrupt EVI loss predated the die-off onset observed in the field by (mean ± SE) 6 ± 1 years. This difference between the year of die-off onset and that of the EVI loss increased as site latitude (r = 0.698), NDVI (r = 0.723) and precipitation of the driest month (BIO14, r = 0.656) did ($p < 0.001$ in all cases), whereas it decreased under warmer and drier conditions (mean maximum temperature, $r = -0.587$; climate water deficit, $r = -0.595$; BIO5, maximum temperature of the warmest month, $r = -0.619$; BIO15, precipitation seasonality, $r = -0.617$; $p < 0.001$ in all cases).

The aridity gradient in the year of abrupt EVI loss reflected a geographical pattern since there was a negative relationship between the site latitude and the year of abrupt EVI loss (Fig. S14). In other words, older droughts, such as that observed in 1985–1986, affected more mountain forests in northeastern Spain, whereas subsequent droughts, such as that observed in 1994–1995, impacted more dryland forests and shrublands in southern and eastern Spain (Fig. S15).

Regarding the last year with negative pointer years, it also predated the die-off onset year by 6 ± 1 years. The difference between the dates of die-off and of the last negative pointer year was negatively related to the site water deficit (Spearman $r_s = -0.424$, $p = 0.004$). In other words, the difference between both dates decreased in the driest sites. For instance, in wet forests with a mean deficit of 20 mm (silver fir, European beech, pedunculated oak, downy oak), this difference was significantly higher (9 ± 2 vs. 4 ± 1 years, $t = 2.376$, $p = 0.020$) than in drier sites with a mean deficit of 55 mm (Scots pine, stone pine, maritime pine, holm oak, Aleppo pine, juniper).

4. Discussion

We deciphered how hotter droughts impact canopy activity and tree growth in die-off hotspots and found, as expected, a greater sensitivity of growth to drought stress than canopy activity. This response may be explained by: (i) the higher noise of relatively coarse (30-m pixels) measures of canopy greenness and cover, often in mixed stands (Leduc et al., 2025), and (ii) the lowest priority of carbon allocation for wood formation, which makes tree rings suitable proxies of water shortage (Babst et al., 2019). Besides, it is important to note that we only considered two widely used vegetation indices, NDVI and EVI, while the use of other indices such as the normalized burn ratio could have revealed different patterns (Leisenheimer et al., 2024).

Climate conditions in the study area are becoming warmer and more arid, leading to hotter droughts (Fig. 1), which have triggered hotspot emergence recently peaking in 1992 and the 2010s. Notably, 2005 stood out as a lethal drought triggering hotspot emergence across Spain (Senf et al., 2020), and it was also highlighted in our selection of hotter droughts. Hotter droughts coincided with abrupt drops in vegetation activity and growth (Fig. 2), as hypothesized, which explains the coupling between the NDVI and growth responses to drought severity,

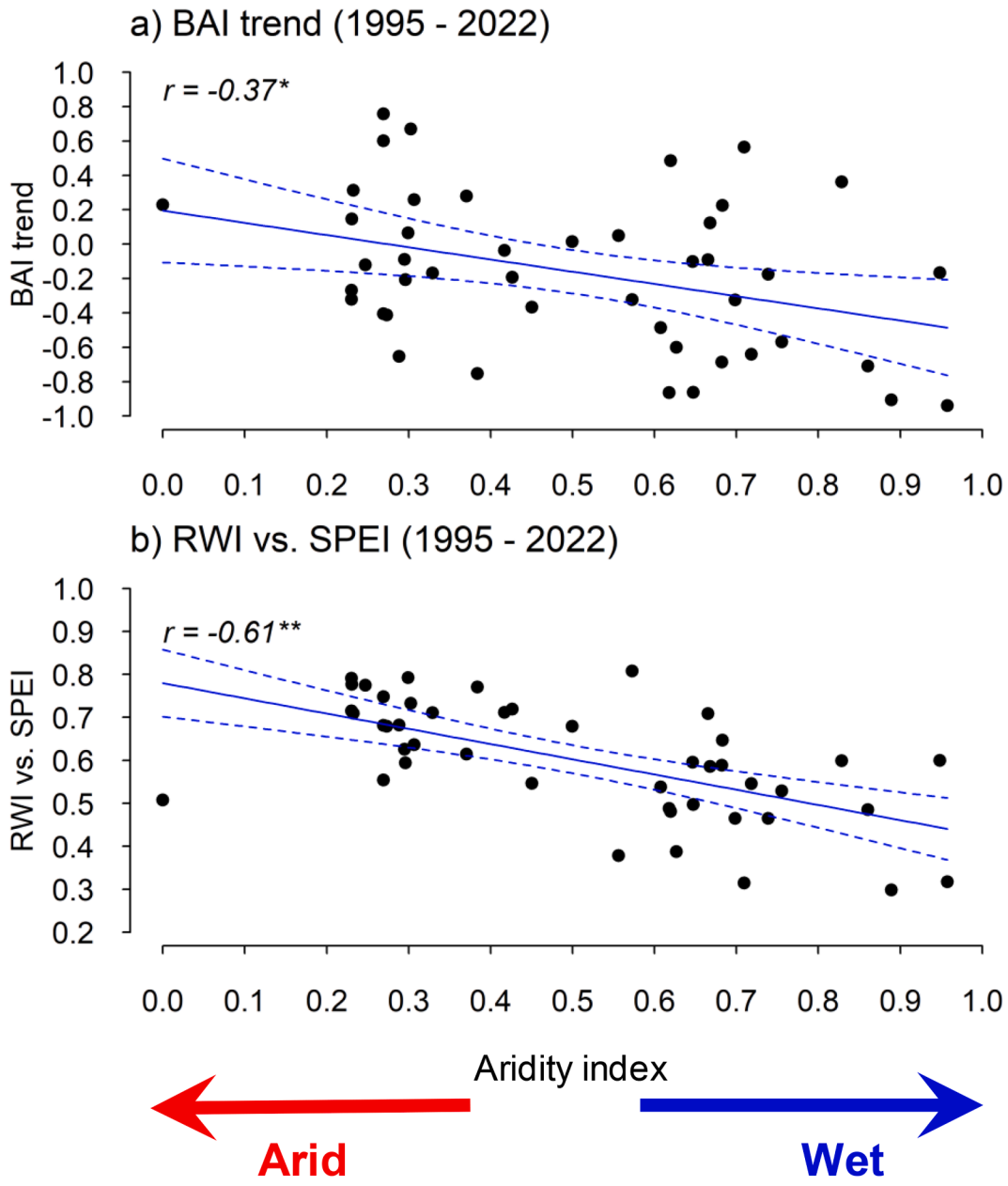

Fig. 3. In the wetter hotspots, growth trends decreased more, whereas growth-drought relationships strengthened in the drier mortality hotspots. (a) Growth (BAI, basal area increment) trends and (b) maximum correlations between ring-width indices (RWI) and the SPEI at 1 to 48-month-long scales as a function of site aridity. The *x* axes show the aridity index (ratio between precipitation and potential evapotranspiration). Pearson correlations are indicated for the linear regressions (blue solid lines) presented in each panel (* $p < 0.05$; ** $p < 0.01$), and the dashed lines show the 95 % confidence intervals.

particularly in drier sites (Figs. 3 and 4). Some studies also found similar spatial coherence on how water shortage constrained canopy activity and growth in dry biomes (Vicente-Serrano et al., 2013), but others reported inconsistent TRW-NDVI relationships in wet biomes due to different phenological timing of leaf flushing and maximum growth rates (Seftigen et al., 2018). Interestingly, we found that TRW and NDVI were more coupled in arid sites which will be in line with the lack of relationship in wet biomes. For example, Nasiri et al. (2025) also found that the relationship between growth variability and vegetation indices depended on the site aridity turning negative as climate conditions became wetter. A caveat to consider is that NDVI and EVI signals retrieved from remote sensing may also include signals from the understory and soil, particularly in the driest sites which showed the lowest cover of the dominant species. In addition, the spatial resolutions of climate, remote sensing and tree-ring data differed, but we are confident they reflected the impacts of regional droughts.

The fact that growth trends were more negative in wetter sites suggests a short but strong response to rare, severe droughts characterized by elevated temperatures, particularly in species sensitive to high VPD such as silver fir (Camarero et al., 2011). In such mesic conditions, growth rates were relatively high and showed an abrupt drop in response to sporadic hotter droughts. Meanwhile, lower slopes in drylands indicate long-term, chronic declines in growth typical of low-productivity sites dominated by resilient pine species (e.g., Aleppo pine) which respond to both atmospheric and soil drought (Gazol et al., 2018). Nevertheless, severe hotter droughts may also surpass the lethal threshold and trigger mortality in drought-tolerant Mediterranean trees (pines) and shrub (junipers) species (Camarero et al., 2015, 2020b, 2026; Valeriano et al., 2021).

Several studies based on vegetation indices and growth data have

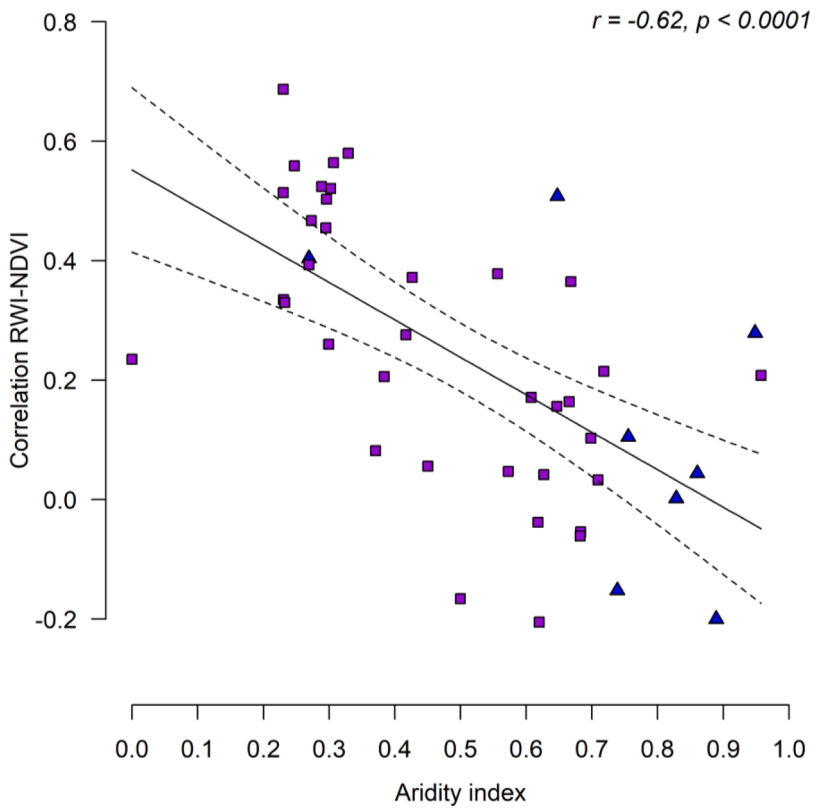

Fig. 4. Negative relationship found between the site aridity index (ratio between precipitation and potential evapotranspiration) and the relationships between canopy activity and growth variability (*r*, Pearson correlation coefficient between mean site NDVI and ring-width index RWI). Squares and triangles show conifers and broadleaves, respectively. The solid line shows the linear regression and the dashed lines show the 95 % confidence intervals.

emphasized the resilience of drought-prone Spanish forests based on greening trends (Gazol et al., 2018; Khoury and Coomes, 2020). Such broad-scale greening has also been highlighted in global studies of mortality sites, which found local drops of NDVI (browning) in hotspots (Yan et al., 2024). In the case of Spain, land-use changes linked to the rapid abandonment of traditional uses in the 1950s and 1960s (logging, grazing) have fueled rapid forest encroachment, explaining greening trends (Infante-Amate and Iriarte-Goñi, 2017). This could have predisposed some hotspots to become more vulnerable to 21st-century hotter droughts by increasing competition for water, but this does not seem to be the case here since many hotspots are sparse stands (Fig. S1; Camarero et al., 2026). In several cases, individual traits such as a smaller stature, lower growth rates, shallow rooting depth or wood traits increasing vulnerability to xylem embolism explain growth decline and tree death (Camarero et al., 2016, 2026; Gazol et al., 2025a). These assessments show that remote sensing imagery must be complemented by field-based, on-ground analyses, including monitoring networks of growth and mortality, which allow capturing the impacts of localized, rare browning hotspots in a greening forest matrix (Gazol and Camarero, 2022; ITN, 2025). Lastly, it should not be forgotten that greening trends do not necessarily involve enhanced forest growth (Correa-Díaz et al., 2019). The uncoupling of canopy and growth may be conditioned by increasing aridity or explained by growth decline and increasing mortality rates reducing forest sensitivity to drought.

It is difficult to find universal common patterns of how trees respond to drought prior to the occurrence of mortality events (Cailleret et al., 2019). The pronounced declines in vegetation activity and growth preceded six years, on average, to the die-off onset. In the case of abrupt growth reductions, they were related to hotter droughts during the past decades and depended on the site water deficit (Figs. 1 and 5). This is the case of the 1986 growth reduction in wet Pyrenean silver fir forests (Camarero et al., 2011) or the 2005 and 2012 droughts in drier Mediterranean pine forests from central and eastern Spain (Camarero et al., 2015; Valeriano et al., 2021). Such lagged responses are expected because growth reductions may occur years before defoliation and mortality are high and affect whole stands (Franklin et al., 1987). For instance, in the Miedes de Aragón *P. pinaster* site, die-off started in 2017, but defoliation and mortality rates continued increasing until 2024 (Camarero et al., 2026). A similar pattern has been observed in some Pyrenean silver fir forests in which browning and mortality of trees has continued since the beginning of the century (Crespo-Antia et al., 2024). This evidences that dating die-off onset is challenging and requires clear criteria based on remote sensing and field data (ITN, 2025). However, we found that growth reductions were common in dry years, and the positive correlation between growth variability and canopy activity increased as aridity did (Fig. 4). Moreover, the difference between the last year of negative pointer years and the die-off year was smaller in drier (4 years) than in wetter sites (9 years) suggesting a higher diagnostic potential of tree-ring series as site aridity increases. These findings contribute to better understand how and when die-off hotspots emerge in response to hotter droughts providing managers useful information on sensitive species (e.g., maritime pine) under specific climatic conditions (hotter droughts). These insights should lead to take adaptive management decisions to improve soil water availability to trees and reduce evaporative demand under intensifying aridity. Future research efforts could also improve hotspot detection using drones and individual growth assessments across global scales to link them with the observed loss of forest resilience (Forzieri et al., 2022).

Finally, two limitations of the analyzed dataset must be acknowledged. First, the 45 study sites were not independent observations; rather, they were grouped sites sharing similar climate histories and species-specific responses which may lead to inflated significance levels. Such pseudoreplication issue cannot be easily solved since the sites' responses to drought, in terms of NDVI, EVI and growth, are distributed

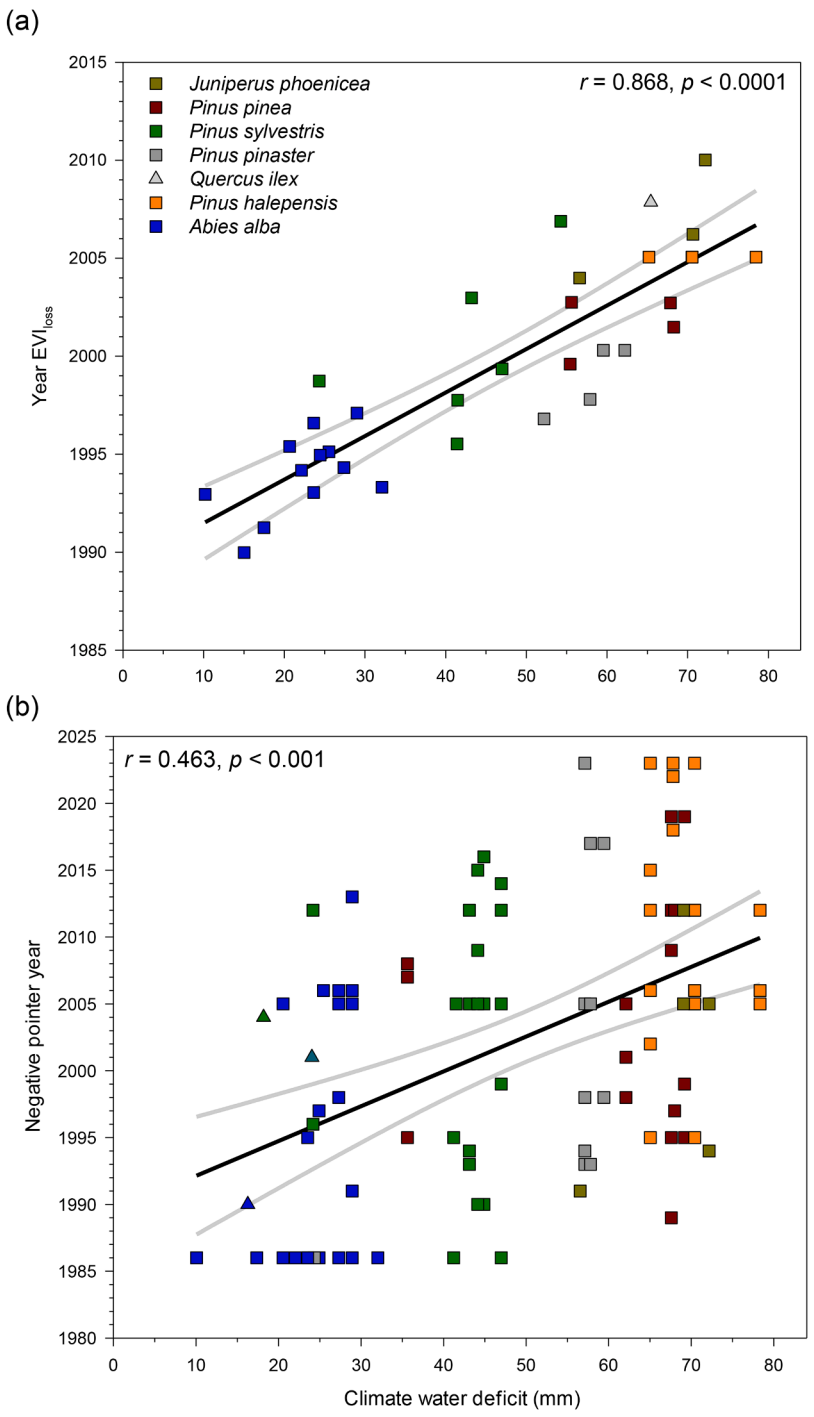

Fig. 5. Positive relationships found between the site climate water deficit (difference between reference and actual evapotranspiration) and (a) the year of abrupt EVI loss or (b) the negative pointer years indicating very low growth rates. Squares and triangles indicate conifers and broadleaves, respectively. Colors indicate species. The black and grey lines show the linear regression and the 95 % confidence intervals, respectively.

along aridity gradients (Fig. S2). Second, our study design did not allow to validate the 6-year lead time between EVI loss and die-off onset on an independent dataset. We acknowledge that without a prospective validation, the 6-year lead time is a diagnostic hindcast, rather than a validated forecast. Furthermore, our data show temporal associations between drought, NDVI-EVI or growth decline, and die-off which could be a consequence of the same stress processes leading to tree death, or, alternatively, they could be independent but correlated responses. Disentangling correlation from causation in similar observational datasets, presenting both spatial and temporal autocorrelation, is challenging and would require additional efforts. Nevertheless, our study also shows that field monitoring of tree defoliation and mortality, particularly in die-off hotspots, are critical to validate remote-sensing information.

5. Conclusions

By integrating remote sensing and dendroecological data across 45 mortality hotspots spanning wide climatic and ecological gradients in Spain, we provide a comprehensive assessment of how hotter droughts reshape forest functioning prior to die-off events. First, die-off and

mortality hotspots were linked to hotter droughts which have become more frequent in the past decades as warmer conditions amplified aridity. Second, growth responded more strongly to drought than canopy activity, despite both response variables covaried. Growth sensitivity to drought intensified toward drier environments, suggesting chronic water limitation amplifies climate–growth coupling. In contrast, wetter forests displayed sharper growth declines, consistent with acute vulnerability to extreme atmospheric drought and limited hydraulic safety margins. Importantly, we document a progressive decoupling between canopy activity and radial growth, signalling an erosion of forest resilience under sustained climatic stress. Third, our ability to detect hotspot occurrence using greenness was poor because years of abrupt EVI loss preceded the years of die-off onset by six years on average. This suggests structural and physiological deterioration may begin long before mortality becomes apparent and die-off hotspots are observed.

Funding

We acknowledge funding from projects PID2021-123675OB-C43 and TED2021-129770B-C21 (Spanish Ministry of Science and Innovation). AP acknowledges funding through a CIHEAM-IAMZ master scholarship. CV and EGA were supported by the Johannes Amos Comenius Programme (P JAC), project No CZ.02.01.01/00/22_008/0004605, Natural and anthropogenic georisks.

CRediT authorship contribution statement

J.Julio Camarero: Writing – original draft, Visualization, Validation, Supervision, Software, Resources, Project administration, Methodology, Investigation, Funding acquisition, Formal analysis, Data curation, Conceptualization. **Antonio Gazol:** Writing – review & editing, Visualization, Validation, Supervision, Software, Project administration, Methodology, Investigation, Funding acquisition, Formal analysis, Data curation, Conceptualization. **Cristina Valeriano:** Writing – review & editing, Visualization, Validation, Software, Resources, Methodology, Investigation, Formal analysis, Data curation. **Michele Colangelo:** Writing – review & editing, Validation, Supervision, Resources, Methodology, Investigation, Data curation. **Manuel Pizarro:** Writing – review & editing, Visualization, Software, Resources, Methodology, Investigation, Formal analysis. **Estér González de Andrés:** Writing – review & editing, Visualization, Validation, Software, Resources, Investigation, Conceptualization. **Arens Pëto:** Writing – review & editing, Visualization, Validation, Software, Methodology, Investigation, Conceptualization.

Declaration of competing interest

The authors declare that they have no known competing financial interests or personal relationships that could have appeared to influence the work reported in this paper.

Acknowledgments

We sincerely thank Paloma Ruiz-Benito (Univ. Alcalá de Henares, Spain) for the coordination of the project PID2021-123675OB-C43, which helped finishing this study. We thank colleagues of several institutions participating in field sampling (Alejandro Cantero, Hazi, Vitoria; Ricardo Díaz Delgado, Estación Biológica de Doñana, CSIC, Sevilla; Juan Carlos Linares, José I. Seco and Raúl Sánchez-Salguero, Univ. Pablo de Olavide, Sevilla; César Morales-Molino, P. Ruiz-Benito, M. A. Zavala, Mariano García-Alonso; Univ. Alcalá; F.J. Gallego, Univ. Complutense, Madrid; Antonio Cachinero and Oscar Pérez-Priego, rSpain Univ. Córdoba).

Supplementary materials

Supplementary material associated with this article can be found, in the online version, at doi:10.1016/j.agrformet.2026.111238.

Data availability

Data will be made available on request.

References

Abatzoglou, J.T., Dobrowski, S.Z., Parks, S.A., Hegewisch, K.C., 2018. Terraclimate, a high-resolution global dataset of monthly climate and climatic water balance from 1958 to 2015. Sci. Data 5, 170191. https://doi.org/10.1038/sdata.2017.191.

Allen, C.D., Breshears, D.D., McDowell, N.G., 2015. On underestimation of global vulnerability to tree mortality and forest die-off from hotter drought in the. Anthr. Ecosph. 6, 1–55.

Babst, F., Bouriaud, O., Poulter, B., Trouet, V., Girardin, M.P., Frank, D.C., 2019. Twentieth century redistribution in climatic drivers of global tree growth. Sci. Adv. 5, eaat4313. https://doi.org/10.1126/sciadv.aat4313.

Beguería, S., Vicente-Serrano, S.M., 2023. SPEI: Calculation of the Standardized Precipitation-Evapotranspiration Index. SPEI. https://doi.org/10.32614/CRAN.package. R package version 1.8.1<. https://CRAN.R-project.org/package=SPEI. >.

Brodribb, T.J., Powers, J., Cochard, H., Choat, B., 2020. Hanging by a thread? Forests and drought. Science 368, 261–266.

Bunn, A.G., 2008. A dendrochronology program library in R (dplR). Dendrochronologia 26, 115–124. https://doi.org/10.1016/j.dendro.2008.01.002.

Bunn, A.G., 2010. Statistical and visual crossdating in R using the dplR library. Dendrochronologia 28, 251–258. https://doi.org/10.1016/j.dendro.2009.12.001.

Bunn, A.G., Korpela, M., Biondi, F., Campelo, F., Klesse, S., Mérian, P., Qeadan, F., Zang, C., 2025. dplR: Dendrochronology Program Library in R. R package version 1.7.8. https://doi.org/10.32614/CRAN.package.dplR. https://CRAN.R-project.org/package=dplR.

Cachinero-Vivar, A.M., Pérez-Priego, O., Camarero, J.J., 2025. Climate drivers of dieback in Mediterranean urban pine forests. Urban For. Urban Green. 112, 128970.

Cailleret, M., Dakos, V., Jansen, S., Robert, E.M., Aakala, T., Amoroso, M.M., Antos, J.A., Bigler, C., Bugmann, H., Caccianiga, M., Camarero, J.J., et al., 2019. Early-warning signals of individual tree mortality based on annual radial growth. Front. Plant Sci. 9, 1964. https://doi.org/10.3389/fpls.2018.01964.

Camarero, J.J., Bigler, C., Linares, J.C., Gil-Pelegrín, E., 2011. Synergistic effects of past historical logging and drought on the decline of Pyrenean silver fir forests. For. Ecol. Manage 262, 759–769.

Camarero, J.J., Gazol, A., Sangüesa-Barreda, G., Oliva, J., Vicente-Serrano, S.M., 2015. To die or not to die: early warnings of tree dieback in response to a severe drought. J. Ecol. 103, 44–57.

Camarero, J.J., Sangüesa-Barreda, G., Vergarechea, M., 2016. Prior height, growth, and wood anatomy differently predispose to drought-induced dieback in two Mediterranean oak species. Ann. For. Sci. 73, 341–351.

Camarero, J.J., Colangelo, M., Gazol, A., Azorín-Molina, C., 2020a. Drought and cold spells trigger dieback in temperate forests. Dendrochronologia 66, 125812.

Camarero, J.J., Gazol, A., Sánchez-Salguero, R., Sangüesa-Barreda, G., Díaz-Delgado, R., Casals, R., 2020b. Dieback and mortality of junipers caused by drought: dissimilar growth and wood isotope patterns preceding shrub death. Agric. For. Meteorol. 291, 108078.

Camarero, J.J., Colangelo, M., Valeriano, C., Gazol, A., González de Andrés, E., Alonso-Forn, D., Voltas, J., Torres-Ruiz, J.M., Delzon, S., Badel, E., Gil-Pelegrín, E., 2026. Xylem pit anatomy and minimum leaf conductance drive drought mortality in *Pinus pinaster*. Plant Cell Env. 49, 279–294. https://doi.org/10.1111/pce.70211.

Correa-Díaz, A., Silva, L.C.R., Horwath, W.R., Gómez-Guerrero, A., Vargas-Hernández, J., Villanueva-Díaz, J., Velázquez-Martínez, A., Suárez-Espinoza, J., 2019. Linking remote sensing and dendrochronology to quantify climate-induced shifts in high-elevation forests over space and time. J. Geophys. Res.: Biogeosciences 124, 166–183. https://doi.org/10.1029/2018JG004687.

Crespo-Antia, J.P., Gazol, A., Pizarro, M., González de Andrés, E., Valeriano, C., Rubio-Cuadrado, A., Linares, J.C., Camarero, J.J., 2024. Matching vegetation indices and tree vigor in Pyrenean silver fir stands. Remote Sens. 16, 4564.

DeSoto, L., et al., 2020. Low growth resilience to drought is related to future mortality risk in trees. Nat. Comm. 11, 545.

Fick, S.E., Hijmans, R.J., 2017. WorldClim 2: new 1-km spatial resolution climate surfaces for global land areas. Int. J. Clim. 37, 4302–4315.

Flood, N., 2013. Seasonal composite landsat TM/ETM+ images using the medoid (a Multi-Dimensional Median). Remote Sens. 5, 6481–6500.

Forzieri, G., Dakos, V., McDowell, N.G., Ramdane, A., Cescatti, A., 2022. Emerging signals of declining forest resilience under climate change. Nature 608, 534–539.

Franklin, J.F., Shugart, H.H., Harmon, M.E., 1987. Tree death as an ecological process. BioScience 37, 550–556. https://doi.org/10.2307/1310665.

Fritts, H.C., 1976. Tree Rings and Climate. Academic Press, London.

Gazol, A., Camarero, J.J., 2022. Compound climate events increase tree drought mortality across European forests. Sci. Tot. Environ. 816, 151604.

Gazol, A., Camarero, J.J., Vicente-Serrano, S.M., Sánchez-Salguero, R., Gutiérrez, E., et al., 2018. Forest resilience to drought varies across biomes. Glob. Chang. Biol. 24, 2143–2158. https://doi.org/10.1111/gcb.14082.

Gazol, A., Pizarro, M., Hammond, W.H., Allen, C.D., Camarero, J.J., 2025a. Droughts preceding tree mortality events have increased in duration and intensity, especially in dry biomes. Nat. Comm. 16, 5779.
Gazol, A., Tamudo, E., Valeriano, C., González de Andrés, E., Colangelo, M., Camarero, J. J., 2025b. A standardized framework to estimate drought-induced vulnerability and its temporal variation in woody plants based on growth. Forests 16, 760.
Greenwood, S., Ruiz-Benito, P., Martínez-Vilalta, J., Lloret, F., Kitzberger, F., et al., 2017. Tree mortality across biomes is promoted by drought intensity, lower wood density and higher specific leaf area. Ecol. Lett. 20, 539–553.
Grossiord, C., Buckley, T.N., Cernusak, L.A., Novick, K.A., Poulter, B., et al., 2020. Plant responses to rising vapor pressure deficit. New Phytol. 226, 1550–1566.
Hammond, W.M., Williams, A.P., Abatzoglou, J.T., et al., 2022. Global field observations of tree die-off reveal hotter-drought fingerprint for Earth's forests. Nat. Comm. 13, 1761. https://doi.org/10.1038/s41467-022-29289-2.
Hijmans, R., 2024. raster: Geographic Data Analysis and Modeling_. R package version 3.6–30. Available online at https://CRAN.R-project.org/package=raster. accessed January 7, 2026.
Hijmans, R.J., Cameron, S.E., Parra, J.L., Jones, P.G., Jarvis, A., 2005. Very high resolution interpolated climate surfaces for global land areas. Int. J. Clim. 25, 1965–1978. https://doi.org/10.1002/joc.1276.
Hijmans, R.J., Barbosa, M., Ghosh, A., Mandel, A., 2024. Geodata: Download Geographic Data_. R package version 0.6–2. https://CRAN.R-project.org/package=geodata. accessed January 7, 2026.
Holmes, R., 1983. Computer-assisted quality control in tree-ring dating and measurement. Tree Ring Bull. 43, 69–78.
Huete, A., 1997. Comparison of vegetation indices over a global set of TM images for EOS-MODIS. Remote Sens. Env. 59, 440–451.
Huete, A., Didan, K., Miura, T., Rodriguez, E.P., Gao, X., Ferreira, L.G., 2002. Overview of the radiometric and biophysical performance of the MODIS vegetation indices. Remote Sens. Env. 83, 195–213.
Infante-Amate, J., Iriarte-Goñi, I., 2017. Las bioenergías en España. Una serie de producción, consumo y stocks entre 1860 y 2010. (No. 1702). Documentos de Trabajo de la Sociedad Española de Historia Agraria. Soc. Esp. Hist. Agrar. available at https://ideas.repec.org/p/seh/wpaper/1702.html accessed 22 March 2022).
ITN, International Tree Mortality Network, 2025. Towards a Global Understanding of Tree Mortality, 245. New Phytol, pp. 2377–2392. https://doi.org/10.1111/nph.20407.
Kennedy, R.E., Yang, Z., Cohen, W.B., 2010. Detecting trends in forest disturbance and recovery using yearly Landsat time series: 1. LandTrendr—temporal segmentation algorithms. Remote Sens. Env. 114, 2897–2910.
Khoury, S., Coomes, D.A., 2020. Resilience of Spanish forests to recent droughts and climate change. Glob. Chang. Biol. 26, 7079–7098.
Leduc, F., Coops, N.C., Morin-Bernard, A., Moreau, G., Achim, A., 2025. A review of dendrochronology and remote sensing integration for forest growth and disturbance monitoring. Curr. For. Rep. 11, 25.
Leisenheimer, L., Wellmann, T., Jänicke, C., Haase, D., 2024. Monitoring drought impacts on street trees using remote sensing - disentangling temporal and species-specific response patterns with Sentinel-2 imagery. Ecol. Inf. 82, 102659. https://doi.org/10.1016/j.ecoinf.2024.102659.
Liu, Y., Kumar, M., Katul, G.G., Porporato, A., 2019. Reduced resilience as an early warning signal of forest mortality. Nat. Clim. Ch. 9, 880–885.
Lu, R., Williams, L.J., Trouvé, R., Murphy, B.P., Baker, P.J., et al., 2026. Pervasive increase in tree mortality across the Australian continent. Nat. Plants 12, 62–73. https://doi.org/10.1038/s41477-025-02188-2.
Martin-Benito, D., Férriz, M., Conde, M., von Arx, G., Fonti, P., Olano, J.M., Gea-Izquierdo, G., 2025. Loss of stomatal regulation sensitivity to CO2 and reduced xylem hydraulic conductivity contribute to long-term tree decline and mortality. Glob. Chang. Biol. 31, e70221. https://doi.org/10.1111/gcb.70221.
Maxwell, R.S., Larsson, L.A., 2021. Measuring tree-ring widths using the CooRecorder software application. Dendrochronologia 67, 125841.
McDowell, N., Pockman, W.T., Allen, C.D., Breshears, D.D., Cobb, N., et al., 2008. Mechanisms of plant survival and mortality during drought: why do some plants survive while others succumb to drought? New Phytol. 178, 719–739.
Mirzabaev, A., Stringer, L.C., Benjaminsen, T.A., Gonzalez, P., Harris, R., Jafari, M., Stevens, N., Tirado, C.M., Zakieldeen, S., 2022. Cross-chapter Paper 3: deserts, semiarid areas and desertification. Climate Change 2022: Impacts, Adaptation and Vulnerability. Cambridge Univ. Press, Cambridge, UK and New York, USA, pp. 2195–2231. https://doi.org/10.1017/9781009325844.020.
Nasiri, V., Hawryło, P., Tymińska-Czabańska, L., Socha, J., 2025. Not always in sync: environmental drivers of the relationship between tree radial growth and vegetation indices in Central Europe. Sci. Tot. Env. 1008, 180969. https://doi.org/10.1016/j.scitotenv.2025.180969.
Pasho, E., Camarero, J.J., de Luis, M., Vicente-Serrano, S.M., 2011. Impacts of drought at different time scales on forest growth across a wide climatic gradient in north-eastern Spain. Agric. For. Meteorol. 151, 1800–1811.
Pizarro, M., 2024. Landsat-based Vegetation Trend in Spain (1984-present). Instituto Pirenaico de Ecología (IPE-CSIC). https://doi.org/10.20350/digitalCSIC/16456.
R Core Team, 2025. R: A Language and Environment for Statistical Computing. R Foundation for Statistical Computing, Vienna, Austria. https://www.R-project.org/.
Roberts, D., Mueller, N., Mcintyre, A., 2017. High-dimensional pixel composites from earth observation time series. IEEE Trans. Geosci. Remote Sens. 55, 6254–6264.
Rouse, J.W., Haas, R.H., Schell, J.A., Deering, D.W., 1974. Monitoring Vegetation Systems in the Great Plains with ERTS, 1. NASA Spec. Publ, p. 309.
Schweingruber, F., Eckstein, D., Serre-Bachet, F., Bräker, U., 1990. Identification, presentation and interpretation of event years and pointer years in dendrochronology. Dendrochronologia 8, 9–38.
Seftigen, K., Frank, D.C., Björklund, J., Babst, F., Poulter, B., 2018. The climatic drivers of normalized difference vegetation index and tree-ring-based estimates of forest productivity are spatially coherent but temporally decoupled in Northern Hemispheric forests. Glob. Ecol. Biogeogr. 27, 1352–1365.
Selke, J., 2025. TerraclimateR: Download Terraclimate Data in Tidy Format. R package version 0.1.0 commit 3075a8247eb6e3fd978d97722ea2107865366500<. https://github.com/julianselke/TerraclimateR. >.
Senf, C., Buras, A., Zang, C.S., Rammig, A., Seidl, R., 2000. Excess forest mortality is consistently linked to drought across Europe. Nat. Comm. 11, 6200. https://doi.org/10.1038/s41467-020-19924-1.
Trugman, A.T., Anderegg, L.D.L., Anderegg, W.R.L., Das, A.J., Stephenson, N.L., 2021. Why is tree drought mortality so hard to predict? Trends Ecol. Evol. 36, 520–532. https://doi.org/10.1016/j.tree.2021.02.001.
Valeriano, C., Gazol, A., Colangelo, M., Camarero, J.J., 2021. Drought drives growth and mortality rates in three pine species under Mediterranean conditions. Forests 12, 1700. https://doi.org/10.3390/f12121700.
van der Maaten-Theunissen, M., van der Maaten, E., Bouriaud, O., 2015. pointRes: an R package to analyze pointer years and components of resilience. Dendrochronologia 35, 34–38. https://doi.org/10.1016/j.dendro.2015.05.006.
van der Maaten-Theunissen, M., Trouillier, M., Schwarz, J., Skiadaresis, G., Thurm, E., van der Maaten, E., 2021. pointRes 2.0: new functions to describe tree resilience. Dendrochronologia 70, 125899. https://doi.org/10.1016/j.dendro.2021.125899.
Vicente-Serrano, S.M., Beguería, S., López-Moreno, J.I., 2010. A multiscalar drought index sensitive to global warming: the standardized precipitation evapotranspiration index. J. Clim. 23, 1696–1718.
Vicente-Serrano, S.M., Gouveia, C., Camarero, J.J., Beguería, S., Trigo, R., López-Moreno, J.I., Azorín-Molina, C., Pasho, E., Lorenzo-Lacruz, J., Revuelto, J., Morán-Tejeda, E., Sánchez-Lorenzo, A., 2013. Response of vegetation to drought time-scales across global land biomes. Proc. Natl. Acad. Sci. USA 110, 52–57.
Wigley, T.M.L., Briffa, K.R., Jones, P.D., 1984. On the average value of correlated time series, with applications in dendroclimatology and hydrometeorology. J. Clim. Appl. Meteorol. 23, 201–213.
Yan, Y., Piao, S., Hammond, W.M., Chen, A., Hong, S., Xu, H., Munson, S.M., Myneni, R. B., Allen, C.D., 2024. Climate-induced tree-mortality pulses are obscured by broad-scale and long-term greening. Nat. Ecol. Evol. 8, 912–923. https://doi.org/10.1038/s41559-024-02372-1.
Zang, C., Biondi, F., 2015. Treeclim: an R package for the numerical calibration of proxy-climate relationships. Ecography 38, 431–436.
Zhu, Z., 2017. Change detection using Landsat time series: a review of frequencies, preprocessing, algorithms, and applications. ISPRS J. Photogramm. Rem. Sens. 130, 370–384. https://doi.org/10.1016/j.isprsjprs.2017.06.013.
Zhu, Z., Woodcock, C.E., 2014. Continuous change detection and classification of land cover using all available Landsat data. Remote Sens. Env. 144, 152–171.
Zomer, R.J., Xu, J., Trabucco, A., 2022. Version 3 of the global aridity index and potential evapotranspiration database. Sci. Data 9, 409. https://doi.org/10.1038/s41597-022-01493-1.
Zscheischler, J., Westra, S., van den Hurk, B.J.M., et al., 2018. Future climate risk from compound events. Nat. Clim. Chang. 8, 469–477.